Cellular uptake and anticancer activity of carboxylated gallium corroles

Melanie Pribisko[a], Joshua Palmer[b], Robert H. Grubbs[a], Harry B. Gray[a,1], John Termini[c,1], and Punnajit Lim[c,1]

[a]Division of Chemistry and Chemical Engineering, California Institute of Technology, Pasadena, CA 91125; [b]Verrix, LLC, Pasadena, CA 91107; and [c]Department of Molecular Medicine, Beckman Research Institute of the City of Hope, Duarte, CA 91010

Contributed by Harry B. Gray, March 1, 2016 (sent for review September 1, 2015; reviewed by David Dolphin and Daniel T. Gryko)

We report derivatives of gallium(III) tris(pentafluorophenyl)corrole, 1 [Ga(tpfc)], with either sulfonic (2) or carboxylic acids (3, 4) as macrocyclic ring substituents: the aminocaproate derivative, 3 [Ga(ACtpfc)], demonstrated high cytotoxic activity against all NCI60 cell lines derived from nine tumor types and confirmed very high toxicity against melanoma cells, specifically the LOX IMVI and SK-MEL-28 cell lines. The toxicities of 1, 2, 3, and 4 [Ga(3-ctpfc)] toward prostate (DU-145), melanoma (SK-MEL-28), breast (MDA-MB-231), and ovarian (OVCAR-3) cancer cells revealed a dependence on the ring substituent: IC_{50} values ranged from 4.8 to >200 μM; and they correlated with the rates of uptake, extent of intracellular accumulation, and lipophilicity. Carboxylated corroles 3 and 4, which exhibited about 10-fold lower IC_{50} values (<20 μM) relative to previous analogs against all four cancer cell lines, displayed high efficacy (E_{max} = 0). Confocal fluorescence imaging revealed facile uptake of functionalized gallium corroles by all human cancer cells that followed the order: 4 >> 3 > 2 >> 1 (intracellular accumulation of gallium corroles was fastest in melanoma cells). We conclude that carboxylated gallium corroles are promising chemotherapeutics with the advantage that they also can be used for tumor imaging.

carboxylated metallocorroles | gallium(III) | corroles | macrocycles | anticancer agents

Corroles are macrocyclic molecules (1) related to porphyrins (2–4) and other aromatic macrocycles whose pharmacological properties have led to the development of many drugs (5, 6). Challenges that must be addressed to realize the full potential of these drugs, however, include synthesis of analogs, determination of pharmacokinetics, targeting, and bioavailability (6, 7). We have taken up the challenge of functionalizing metallocorroles to enhance cell permeability (8, 9). We hope to achieve this goal while still retaining the inherent therapeutic properties of these macrocyclic compounds.

Corroles have received a great deal of attention in recent years (10–13), owing to dramatic advances in methods for their preparation (14–31). Of interest here is a gallium(III) complex, **1** [Ga(tpfc)] (32–35), where tpfc represents the trianion of 5,10,15-tris(pentafluorophenyl)corrole [H_3(tpfc)]. **1** is highly fluorescent, with an emission quantum yield far exceeding that of its zinc porphyrin analog (36–38). The macrocyclic ring of this complex can be selectively modified to afford molecules that exhibit a wide range of physical and chemical properties (1). Previous work focused on a sulfonic acid derivative of Ga(tpfc), **2** [Ga(2,17-S_2tpfc)]; notably, **2** possessed potent antitumor activity both in vitro (using human cancer cells) and in vivo (using murine model animals), making it a powerful reagent for both imaging and therapeutic targeting of cancer cells (39, 40). Additional studies on the mechanism of cytotoxicity demonstrated that numerous cancer cell lines rapidly take up **2** in vitro and induce cell cycle arrest at late M phase (41, 42). Replacement of bis-sulfonic acids with *para*-pyridinium substituents (**5**) was shown to improve uptake and activity, whereas *ortho*-pyridinium substitution (**6**) completely ablated toxicity, indicating that functional group modifications of the corrole can have profound effects on biological activity (41).

To examine the effect of functional group substitution on the cell permeability and cytotoxic activity of corroles, we have expanded our earlier work on **1**; specifically, we have introduced various substituents and examined cellular uptake and anticancer activity of several derivatives. Compound **1** is treated with sulfonic acid to generate **2**, with aminocaproic acid to generate carboxylic acid **3**, or with phosgene to generate **4**. We report that enhanced corrole potencies and intracellular uptakes are dependent upon functional group substitution, and that selectively functionalized corroles can augment anticancer activity by altering cell membrane permeability.

Results and Discussion

Synthesis of Gallium Corroles. **1** (32), **2** (33), and **4** (34) were obtained via literature methods, and molecular masses were confirmed by MALDI-TOF mass spectrometry (Fig. 1). The aminocaproate-substituted corrole **3** was synthesized in 37% yield by nucleophilic aromatic substitution of a *para*-fluoro substituent on the pentafluorophenyl ring of **1** with a substoichiometric amount of 6-aminocaproic acid in anhydrous dimethyl sulfoxide (DMSO) with 1% anhydrous pyridine at 100 °C (Scheme 1). This synthesis followed procedures that have been used to prepare amine-substituted corroles (43). These reactions are highly selective in that only the *para*-fluoro substituent undergoes substitution.

Although preparation of **4** requires phosgene and can only be performed on the metallated corrole (34), **3** can be synthesized using either metallated or free base corrole and does not require harsh reagents. Compound **3** is a promising candidate for both imaging applications and potential development as

Significance

Corroles are macrocyclic molecules related to porphyrins that exhibit intense light absorptions in the visible region. They also are very bright emitters, with luminescence quantum yields over 50% in some cases. Importantly, we have discovered that two corroles functionalized with carboxylate groups at different ring locations exhibit anticancer activity superior to cisplatin. Although the synthetic route to direct carboxylation of the tetrapyrrolic framework requires the use of phosgene, installing aminocaproate on the fluorophenyl ring by nucleophilic aromatic substitution uses mild conditions with biocompatible reagents, requiring only simple purification and providing ready access to structurally complex corroles. Carboxylated corroles are very rapidly taken up by cells, with an order of magnitude gain in dark cytotoxicity likely owing to greater cell permeability.

Author contributions: M.P., J.P., R.H.G., H.B.G., J.T., and P.L. designed research; M.P. and P.L. performed research; M.P. and P.L. contributed new reagents/analytic tools; M.P., J.T., and P.L. analyzed data; and M.P., J.P., R.H.G., H.B.G., J.T., and P.L. wrote the paper.

Reviewers: D.D., University of British Columbia; and D.T.G., Polish Academy of Sciences.

The authors declare no conflict of interest.

[1]To whom correspondence may be addressed. Email: hbgray@caltech.edu, JTermini@coh.org, or PLim@coh.org.

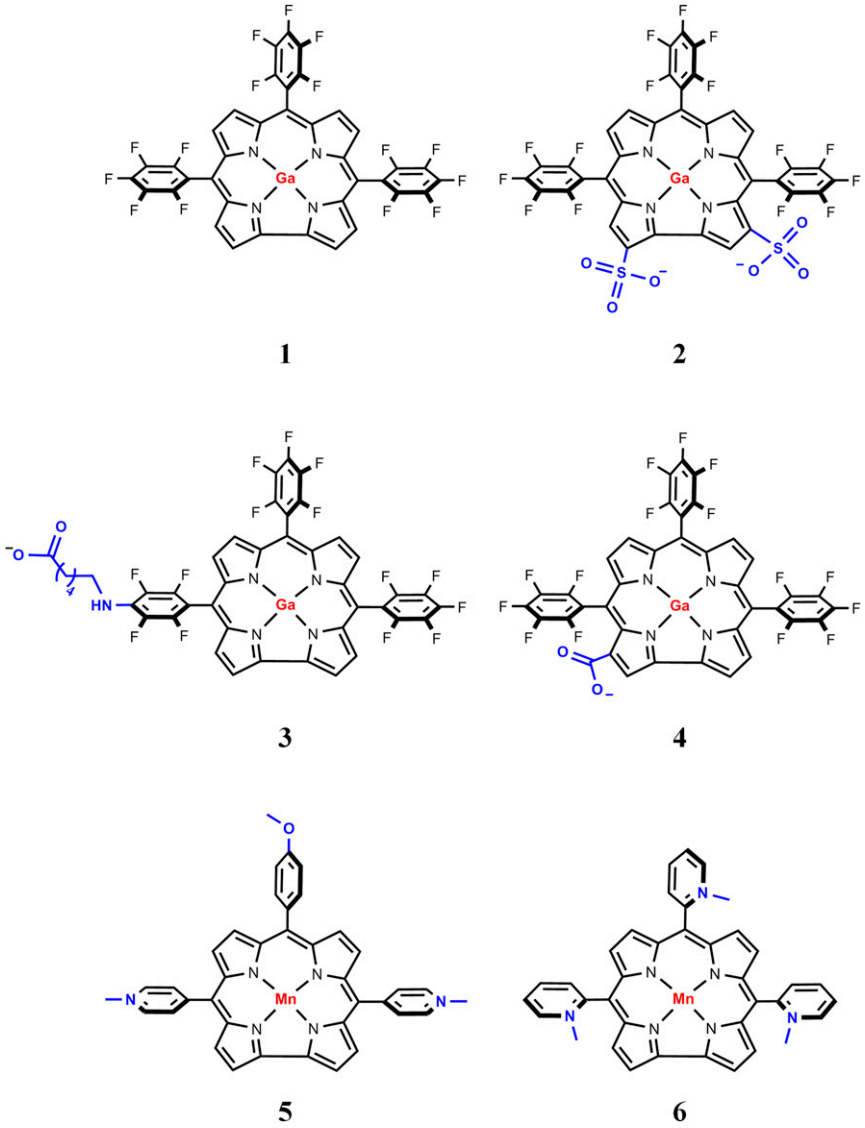

Fig. 1. Structures of functional group-substituted derivatives of corroles. For clarity, the axial pyridine is not shown in the structures.

a chemotherapeutic, as it is easily solubilized in water, and easily prepared and purified.

Modulation of Cytotoxicity by Substituents on the Corrole Ring. The effects of bis-sulfonate, carboxylate, and aminocaproate ring substituents on gallium corrole cytotoxicities were examined using four human cancer cell lines, representing tumors of different origin selected (44) based on previously described sensitivities (41). Each cell line, DU-145 (prostate), SK-MEL-28 (melanoma), MDA-MB-231 (breast), or OVCAR-3 (ovarian), was incubated in growth medium with varying concentrations of **1**–**4** at 37 °C for 72 h in the dark, and the cytotoxicity as a function of concentration was measured using the MTS assay. Dose–response curves are shown in Fig. 2.

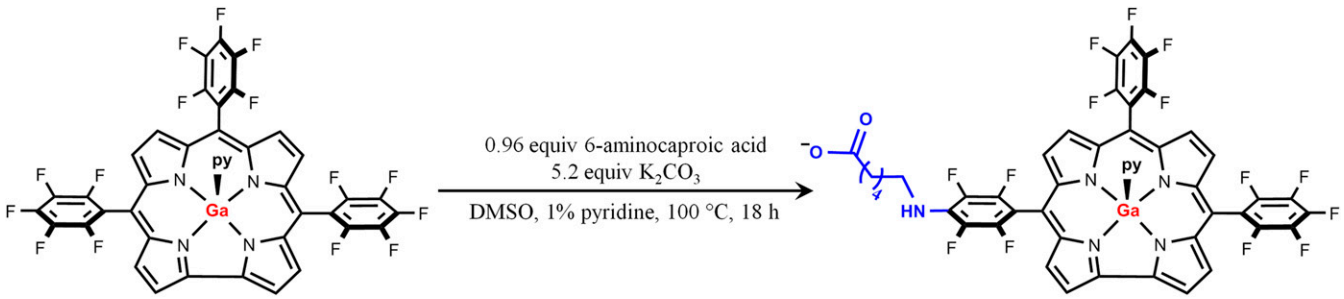

Scheme 1. Synthetic scheme for **3** [Ga(ACtpfc)]. Reagents and conditions: 6-aminocaproic acid, K_2CO_3, DMSO, 1% pyridine, 100 °C, 18 h.

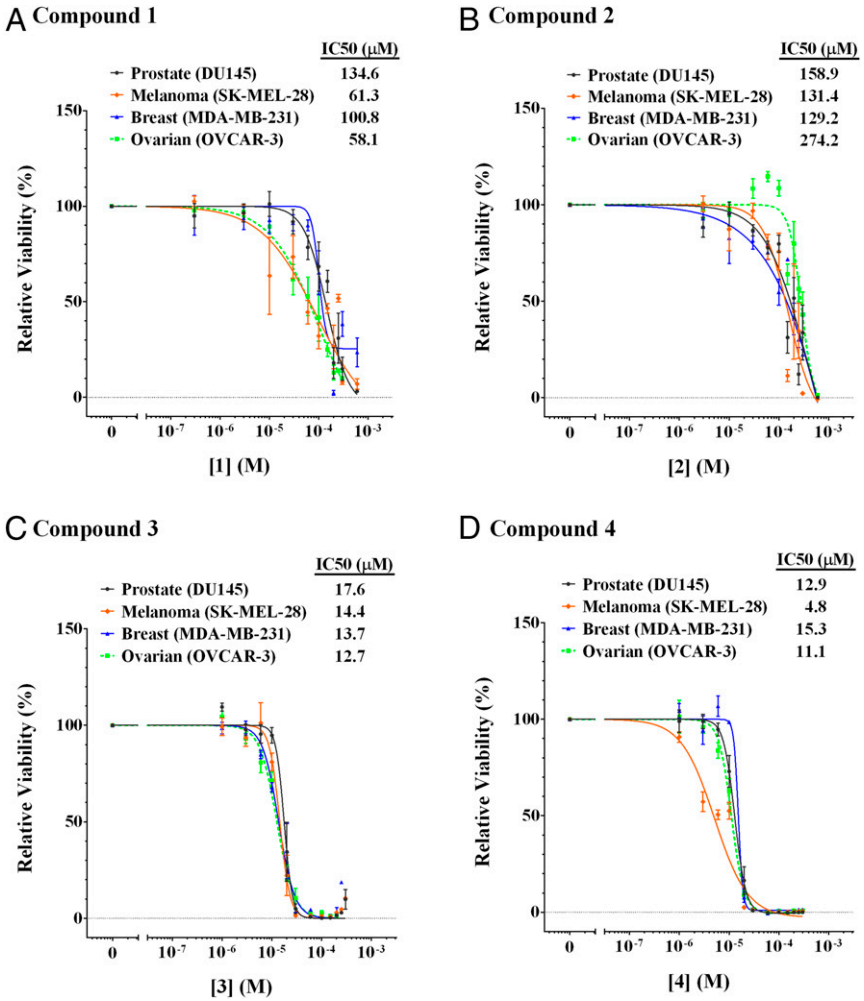

Fig. 2. Cytotoxic effects of functionalized gallium(III) corroles on human cancer cells. Dose–response curves for a 72-h exposure of human tumor cell lines, prostate (DU-145), melanoma (SK-MEL-28), breast (MDA-MB-231), and ovarian (OVCAR-3) to (*A*) **1**, (*B*) **2**, (*C*) **3**, or (*D*) **4** were evaluated using the MTS assay. The viability of each corrole-treated cell line is expressed as a percentage of untreated control growth. A sigmoidal dose–response curve was fitted to the data using GraphPad Prism 6. Data represent the mean ± SD of three independent experiments.

IC_{50} values ranged from 4.8 to 17.6 μM with carboxylated corroles **3** and **4**; these corroles had the highest anticancer activities against all cell lines (Fig. 2 and Table 1). In particular, **4** displayed promising activity against the SK-MEL-28 melanoma line, with an IC_{50} value of 4.8 μM. The cytotoxicities of the carboxylated corroles toward all cell lines were nearly identical, except for **4** in SK-MEL-28 cells, with IC_{50} values in the range of 10–20 μM (Fig. 2 and Table 1), or about 10-fold lower against the same cell lines relative to **1** and **2**. With the exception of the activity of **1** against SK-MEL-28 and OVCAR-3 cell lines, with IC_{50} values of 61.3 and 58.1 μM, respectively (Table 1), the IC_{50} values of **1** and **2** had values ranging from 100 to 274 μM. The order of magnitude improvement in IC_{50} against SK-MEL-28 results from substitution with a single carboxylic acid at the 3 position of **1**, lowering the IC_{50} of **4** to 4.8 μM (Fig. 1 and Table 1). Against the prostate cancer cell line DU-145, bis-sulfonated **2** displayed an IC_{50} of 159 μM, whereas the carboxylated analog **4** was ∼12-fold lower (12.9 μM). In general, the bis-sulfonated corroles were the least effective against all tested cell lines, with the lowest observed IC_{50} values (∼130 μM) against the melanoma line SK-MEL-28 and breast cancer cell line MDA-MB-231. This finding contrasts with that for monocarboxylated **3** and **4** corroles, which displayed IC_{50} values of <20 μM against all cell lines tested, with markedly good activities against SK-MEL-28 and OVCAR-3 lines. The mean IC_{50} values for all carboxylated corroles (12.8 ± 1.3 μM) revealed twofold to threefold higher potency than that reported for cisplatin [46.4 ± 12.4 μM (45) and 39 μM (46)] in MDA-MB-231 cells. Although the IC_{50} values are similar for the carboxylated Ga(III) corroles, data in Table 1 suggest that **4** possesses somewhat greater potency relative to aminocaproate analog **3**.

Although the IC_{50} value is typically the principal metric for the effectiveness of a potential drug, other parameters involving the slope of the dose–response curve (Hill slope, $|\gamma|$) and the maximum effect (E_{max}), which represent the compound's range of useful concentrations and efficacy, respectively, also should be considered in evaluating drug response (47, 48). For example, a drug with low efficacy may only kill 20% of cells even at the highest doses ($E_{max} = 0.8$), or a drug could have a shallow dose–response curve ($|\gamma| < 1$), meaning that the therapeutic benefit or cytotoxic effect may not increase substantially as the maximum tolerated dose is approached. The effectiveness of **1**–**4** was further evaluated by these additional parameters; and the data revealed considerably steep slopes ($|\gamma| \geq 1.0$) for all derivatives in all cell lines tested, with values ranging from 0.9 to 9.7 (Fig. 2 and Table 1). The steep slopes of the dose–response curves were indicative of homogeneous cell populations with highly uniform drug responses (47). The mean slopes for carboxylated corroles

Table 1. Dose–response parameters for gallium corroles

Compound	Cells*	IC_{50}†	±SE	Slope (γ)‡	±SE
1	DU-145	134.6	10.9	−2.1	0.3
	SK-MEL-28	61.3	9.9	−0.9	0.1
	MDA-MB-231	100.8	6.8	−5.7	3.9
	OVCAR-3	58.1	7.2	−1.1	0.2
2	DU-145	158.9	16.2	−1.6	0.3
	SK-MEL-28	131.4	18.5	−2.0	0.5
	MDA-MB-231	129.2	13.2	−1.3	0.2
	OVCAR-3	274.2	15.5	−3.7	0.9
3	DU-145	17.6	0.8	−5.3	1.1
	SK-MEL-28	14.4	0.7	−4.2	0.5
	MDA-MB-231	13.7	1.0	−2.7	0.4
	OVCAR-3	12.7	0.6	−2.5	0.2
4	DU-145	12.9	0.5	−3.9	0.4
	SK-MEL-28	4.8	0.3	−1.4	0.1
	MDA-MB-231	15.3	2.0	−9.7	4.8
	OVCAR-3	11.1	0.4	−3.5	0.4

*Human cancer cells were exposed to each compound for 72 h. Data represent the mean of three independent experiments.
†IC_{50} values are reported in micromolar concentration.
‡Hill slopes (γ) are unitless.

3 and **4** (4.2 ± 0.9) were about twofold steeper than those for **1** (2.5 ± 1.1) and **2** (2.2 ± 0.5), suggesting that the cytotoxic effects or therapeutic benefit of the carboxylated derivatives will increase substantially as the maximum tolerated dose is approached.

The quantifying maximal effect parameter (E_{max}) revealed high compound efficacy for **1**–**4**, except for **1** in MDA-MB-231 cells (Fig. 2). In general, E_{max} is defined between 1 at low doses and 0 at high doses, which corresponds to 100% cytotoxicity (48). With the exception of **1** in MDA-MB-231 cells ($E_{max} = 0.25$), the maximum cytotoxic effect for all compounds tested was ≤0.02, indicating high efficacy (Fig. 2). The lower efficacy of **1** in MDA-MB-231 cells may be explained in part by the "fraction kill" theory, which proposes that inhibitors of cell cycle progression, such as paclitaxel and docetaxel, kill only the subset of cells that pass through S or M phases in the presence of the drug (49, 50). Therefore, cells with substantially longer doubling times, and thus smaller mitotic and S-phase fractions, would have higher values for E_{max} (48). Because gallium corroles were previously shown to arrest cells at the late M phase (41) and the doubling time of MDA-MB-231 cells [population doubling time (PDT), 41.9 h] is considerably longer than DU-145 (PDT, 32.3 h), SK-MEL-28 (PDT, 35.1 h), and OVCAR-3 (PDT, 34.7 h) cells, the reduced mitotic or S-phase fractions of MDA-MB-231 cells that are susceptible to drug-induced toxic effect could account for the lower efficacy ($E_{max} = 0.25$) observed for **1** in MDA-MB-231 cells (Fig. 2). Although correlation of E_{max} with cell proliferation rate has often been shown for cell cycle inhibitors (48), the fraction kill theory does not always apply. For instance, Oxamflatin and NSC663284, which arrest cells at both G_1 and G_2/M, exhibit high efficacy ($E_{max} = 0$) in all 64 breast cancer cell lines tested with varying cell proliferation rates. In summary, **1** and its derivatives, with the exception of **1** in MDA-MB-231 cells, were effective in killing 100% of cancer cells at the highest doses.

Uptake of Ga(tpfc) Derivatives. The intense fluorescence of gallium corroles was exploited to examine intracellular accumulation using confocal microscopy and ImageXpress^{ultra} analysis to measure the rate of uptake of differentially substituted derivatives across all cell lines. Avidity of cellular uptake can influence the observed cytotoxicity of corroles, as we have previously described (41). Confocal image analysis was performed on DU-145 (prostate), SK-MEL-28 (melanoma), MDA-MB-231 (breast), or OVCAR-3 (ovarian) cells incubated with 3 μM **1**, **2**, **3**, or **4** in complete or unsupplemented media for 3 h in the dark; representative images are shown for DU-145 cells (Fig. 3). The nuclei and plasma membranes of cells were visualized by labeling with DAPI (blue fluorescence) and wheat germ agglutinin (WGA)–Alexa Fluor 488 conjugate (green fluorescence), which bind to nuclear DNA and *N*-acetylglucosamine, respectively. Gallium corroles were readily observable in situ as red fluorescence of varying intensities in cells treated with **2**, **3**, and **4**; in contrast, red fluorescence was absent in untreated cells (Fig. 3). In cells treated with 3 μM **1** for 3 h, red fluorescence was not apparent (data not shown), whereas analysis of cellular uptake kinetics revealed that less than 5% of cells were able to internalize **1** at this time point (Fig. 4*A*). The intensities of red fluorescence were much greater in cells exposed to **2** and **4** compared with **3**, even though the IC_{50} of **3** is about the same as **4** and 10-fold lower than **2** (Fig. 3 and Table 1). The standard curves of corrole fluorescence versus compound concentration generated for **1** and its derivatives differed significantly, most likely owing to differences in quantum yields, absorption cross-sections, and solubilities (data not shown); these data confirmed that fluorescence intensity measurements cannot be used to predict or directly compare the intracellular concentrations of different gallium corroles. However, the relative intracellular concentrations of a single compound can be assessed by its fluorescence intensity and compared among different cell lines. Data obtained from confocal image analysis verified that intracellular uptake of **1**–**4** can be monitored by fluorescence microscopy for all cell lines tested.

To quantify the kinetics of intracellular uptake and accumulation of each **1** derivative, ImageXpress^{ultra}, a laser point-scanning confocal microscope, was used for analyses. Cellular uptake of **1**–**4** was assessed in human cancer cell lines DU-145 (prostate), SK-MEL-28 (melanoma), MDA-MB-231 (breast), or OVCAR-3 (ovarian) at a final concentration of 30 μM. Cells were incubated at 37 °C in the dark for 0.25, 1, 3, or 24 h. Results are presented in Fig. 4 *A*–*D* for **1**, **2**, **3**, and **4**, respectively. Each graph indicates the percentage of cells with observable red/corrole fluorescence (*y* axis) versus incubation time (*x* axis) and the median relative fluorescence intensity (RFU), which is directly proportional to the amount of intracellular accumulation (*z* axis). Functional group substitution of **1** resulted in significant differences in the rate of uptake, as follows: **4 >> 3 > 2 >>1** (Fig. 4 *A*–*D*). Within 15 min, **4** fluorescence was observable in ∼80% of ovarian cancer cells, 97% of breast cancer cells, and >99% of prostate cancer and melanoma cells (Fig. 4*D*), whereas up to 3 and 24 h were required to label >80% of cells from all four cancer lines with **3** and **2**, respectively (Fig. 4 *B* and *C*). For **1**, significant uptake (≥80% cells) in melanoma, ovarian, and breast cancer cell lines required 24 h. The uptake of **1** was quite slow in prostate cancer cells, as <5% of cells displayed red fluorescence after 3 h and only about 50% of cells were positive for corrole after incubation for 24 h (Fig. 4*A*). In the case of **4** in DU-145, SK-MEL-28, and OVCAR-3 cells (Fig. 4*D*), as well as **3** in OVCAR-3 cells (Fig. 4*C*), the proportion of corrole-positive cells decreased from nearly 100% at 3 h to about 30–75% at 24 h. Less than 30% of the average numbers of cells analyzed for each cell line was available for the analysis of corrole uptake in these cases; these decreases could result from the cytotoxicity of **3** and **4** following 24 h of incubation. As a result, analysis of uptake among the surviving subpopulation revealed an ostensibly lower proportion of corrole-positive cells.

Intracellular accumulation, which correlates with the median RFU, was compared among the four human cancer cell lines and revealed the most efficient uptake of **1**–**4** into melanoma (SK-MEL-28) cells (Fig. 4 *A*–*D*). After 3 h of incubation, the

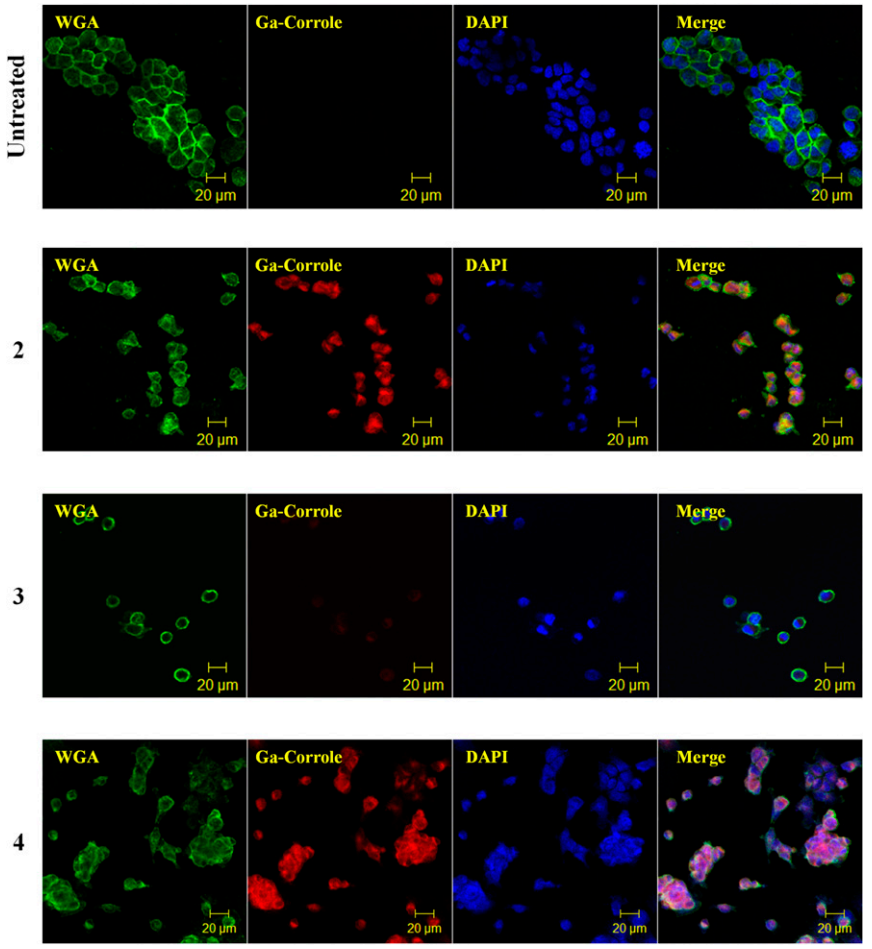

Fig. 3. Intracellular uptake of functional group-substituted derivatives of **1** [Ga(tpfc)]. Prostate cancer cells (DU-145) were treated with 3 μM **2**, **3**, **4** for 3 h or untreated (medium only). Cells were labeled with WGA conjugated to Alexa Fluor 488 and DAPI. Images were obtained at 40× magnification using an upright confocal microscope and displayed in three-color channels with a merged image. Fluorescence settings were kept constant between imaging, and images were captured at fixed exposure and gain settings. (Scale bar: 20 μm.)

fluorescence of **4** was approximately twofold to threefold higher in melanoma cells compared with prostate, breast, and ovarian cancer cells (Fig. 4*D*). A twofold enhancement of fluorescence in melanoma cells compared with the other three cell lines was observed for **1**, **2**, and **3** after 24 h (Fig. 4 *A*–*C*). The most efficient uptake of gallium corroles into melanoma (SK-MEL-28) cells has been proposed to be consistent with transferrin-mediated transport (41), because these cells are well known to avidly accumulate iron via this mechanism (51, 52). The exceptional efficiency of gallium corrole uptake and intracellular accumulation in melanoma cells correlates with an observable increase in cytotoxic activity against these cells over other cell lines for **1** and **4** (Figs. 2 and 4 and Table 1); but for **2** and **3**, the cytotoxic activity is similar among all cell lines and does not correlate with the accumulated corrole levels (Figs. 2 and 4 and Table 1). Overall, excellent kinetics of intracellular uptake and accumulation, especially in melanoma cells, were found for **3** and **4**, suggesting that substitution with carboxylic acid or aminocaproic acid increases cell permeability.

The mechanisms of uptake of gallium corroles, and macrocyclic compounds in general, into cancer cells remain elusive, and factors that control cell permeability are mostly unknown (5, 7). Recent research in drug discovery and development (7) has focused on altering the physical and chemical properties of macrocycles in attempts to improve cell permeability (5, 53). Some chemical properties that have been shown to enhance cell permeability and uptake include lower molecular weight (M_r), smaller polar surface area (tPSA), and higher calculated lipophilicity (cLogP) (5). Predictions of tPSA and cLogP were made for substituted derivatives **2**, **3**, and **4**, using ChemDraw (Table 2). The carboxylated corroles, **3** and **4**, with enhanced cellular uptake, cell permeability, and potency relative to bis-sulfonated **2**, showed lower M_r, smaller tPSA, and increased cLogP (Table 2).

Profile of 3 [Ga(ACtpfc)] Sensitivity in a NCI60 Cell Panel. In view of the promising results observed for carboxylated corroles, **3** was selected for expanded cell screening to uncover additional susceptible cancer cell lines. The cytotoxic activity of **3** was tested at a dose of 10^{-5} M against 60 human cancer cell lines representing nine distinct tumor types in the anticancer screening program of the National Cancer Institute (NCI). The in vitro parameters for cytotoxicity, growth percent, and lethality were obtained for **3** and reported as a mean graph of the percent growth of treated cells (Fig. 5). Bars in the mean graph depict the deviation of individual tumor cell lines from the overall mean value for all cells tested. Bars that project to the right of the mean represent cell lines that are more sensitive to **3**, whereas cell lines less sensitive to the compound display bars that project to the left.

The numerical values associated with this assay represent growth relative to the no-drug control and the numbers of cells at time 0 (Fig. 5). This allows detection of both growth inhibition

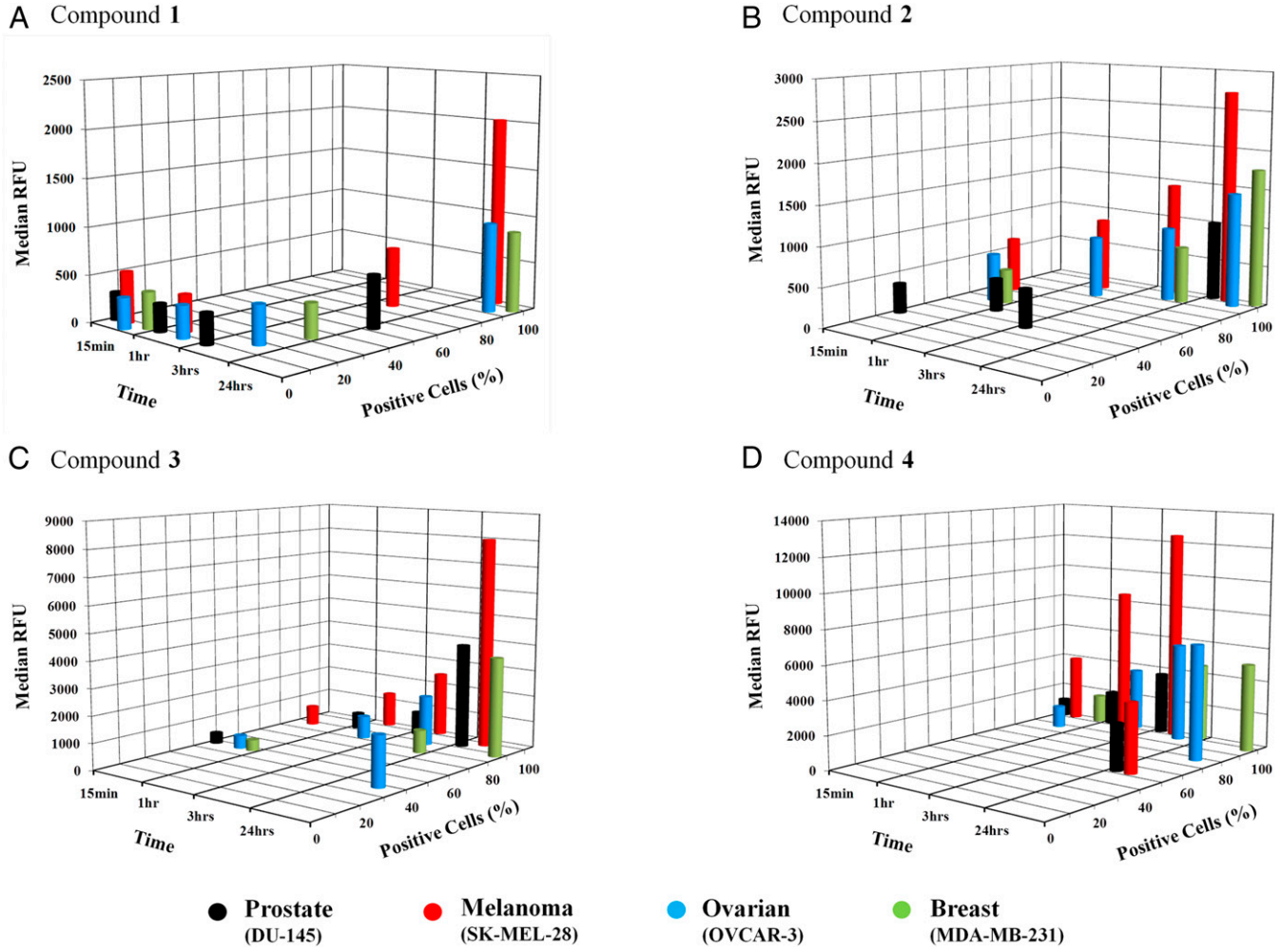

Fig. 4. Kinetics of intracellular uptake and accumulation of **1** and its derivatives by DU-145 (black), SK-MEL-28 (red), OVCAR-3 (blue), and MDA-MB-231 (green) cancer cells were determined using the ImageXpress^{ultra} system. Cells were treated with 30 μM (*A*) **1** [Ga(tpfc)], (*B*) **2** [Ga(2,17-S_2tpfc)], (*C*) **3** [Ga(ACtpfc)], or (*D*) **4** [Ga(3-ctpfc)] for the amount of time indicated on the *x* axis. The *y* axis represents a percentage of corrole-positive cells with observable intracellular red fluorescence. The extent of corrole uptake and intracellular accumulation was directly proportional to the median fluorescence intensity (RFU) on the *z* axis. Cell images were obtained at 20× magnification using filters for blue (DAPI) and red fluorescence.

(values between 0 and 100) and lethality (values less than 0). For example, a value of 100 signifies no growth inhibition, 40 means 60% growth inhibition, 0 means no net growth over the course of the experiment, −40 means 40% lethality, and −100 indicates all cells are dead. The percentage of growth inhibition and lethality resulting from **3** is given in Table 3. In most cell lines, inhibition of cell proliferation was observed ranging from 30% to 99% following exposure to 10 μM **3** for 48 h, with an average growth inhibition of 70%. Growth inhibitions reflect cytostatic activity of the compound as previously shown for **2** (41). In contrast, cell lethality is only evident in melanoma cells, specifically the LOX IMVI and SK-MEL-28 cell lines. Overall, **3** is highly active against all NCI60 cell lines derived from nine tumor types (Table 3), suggesting that carboxylated gallium corroles are effective, cell-permeable chemotherapeutic agents.

Table 2. Chemical properties of functional group substituted 1 [Ga(tpfc)]

Compounds	M_r^*	tPSA†	cLogP‡
2	1,021.30	135.9	9.6
3	974.37	62.0	13.5
4	907.21	58.8	13.1

ChemBioDraw Ultra (version 13.0.2.3021).
*Molecular weight.
†Calculation of polar surface area based on fragment contributions.
‡Calculated logP based on Biobyte algorithm.

Conclusions

Gallium corroles with different ring substituents exhibited variable uptake rates and cytotoxic activity against numerous human cancer cell lines. The uptake, intracellular accumulation, and potency (IC_{50}) varied by compound: carboxylated derivatives **3** and **4** augmented cell permeability, as revealed by enhanced uptake rates, and increased intracellular accumulation, resulting in higher potency compared with **1** and **2**. The carboxylated corroles exhibited strong cytotoxic effects in prostate, melanoma, breast, and ovarian cancer cells; the effective cytotoxic dose (<20 μM) was lower than that of a widely used chemotherapeutic agent, cisplatin (45, 46), as well as those of other gallium compounds under study as therapeutic agents (54–56). Compound **4** was exceptionally active as a cytotoxic agent against melanoma SK-MEL-28 cells (IC_{50} = 4.8 μM); notably, >99% of cells exhibited intracellular corrole accumulation within 15 min. In comparison with **2**, derivatives **3** and **4** have lower molecular

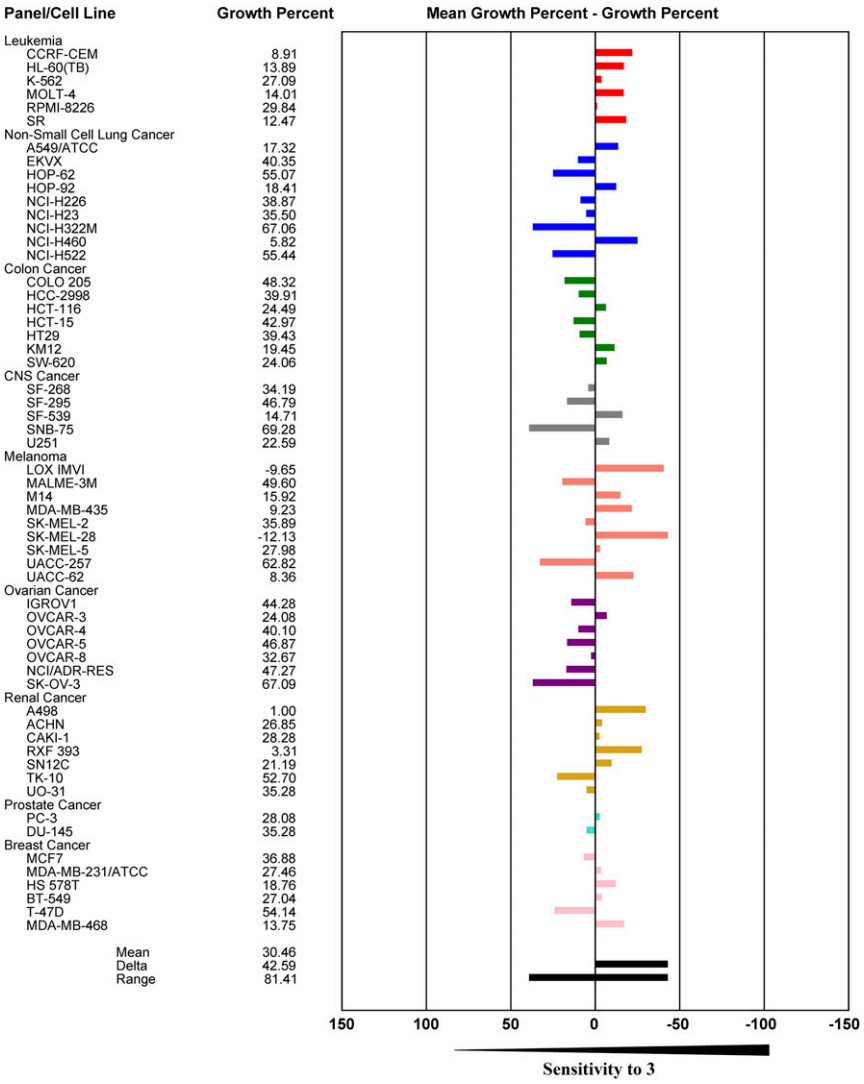

Fig. 5. Mean graph representation of growth inhibition effects of **3** [Ga(ACtpfc)]. Carboxylated gallium corrole submitted to the NCI screen were evaluated against 60 human tumor cell lines. Growth percent and lethality were obtained at a single dose (10^{-5} M) of **3** and the mean growth percent across all 60 cell lines was calculated. The individual response of each cell line to the compound is depicted by a bar graph extending either to the right or left of the mean. Bars projecting to the right represent cell lines that are more sensitive than average, whereas less sensitive cell lines show bars projecting to the left. The length of each bar is proportional to the relative sensitivity compared with the mean determination. The graph was color-coded by tissue of origin: red, leukemia cell line; blue, lung cancer; green, colon cancer; gray, CNS cancer; coral, melanoma; purple, ovarian cancer; gold, renal cancer; turquoise, prostate cancer; pink, breast cancer.

weights (M_r), smaller polar surface areas (tPSA), and higher calculated lipophilicities (cLogP), all chemical properties associated with enhanced cell permeability and uptake (5). The carboxylated corroles also displayed high efficacy in cell killing and a highly homogeneous cytotoxic response within each cell population.

Because the synthesis of **3**, which has anticancer activity close to that of **4**, does not require the use of harsh reagents, it represents an easily and safely prepared anticancer lead that also can function as a fluorescence imaging agent.

Materials and Methods

Materials. **1**, **2**, and **4** were prepared by literature methods (Fig. 1) (32–34). The synthesis and characterization of compound **3** (Scheme 1) proceeded as follows: a round-bottom flask was charged with **1** (20.0 mg, 0.025 mmol), 6-aminocaproic acid (3.1 mg, 0.024 mmol), and K_2CO_3 (18.0 mg, 0.13 mmol) under argon. To this mixture was added anhydrous DMSO (0.5 mL) and anhydrous pyridine (1%). The reaction mixture was heated to 100 °C and stirred for 18 h, after which it was cooled and then diluted with $CHCl_3$ (10 mL), washed sequentially with H_2O (4 × 10 mL) and brine (1 × 10 mL), and then dried over Na_2SO_4. The solvent was removed in vacuo, and the crude residue was purified by flash chromatography [SiO_2, 1% pyridine, 0–10% (vol/vol) MeOH in CH_2Cl_2] to provide 9.1 mg (37%) of monocarboxylate as a purple solid. Characterization of **3** was performed using $^1H/^{19}F$ NMR spectroscopy and MALDI-TOF mass spectrometry, although these techniques did not distinguish between regioisomers with monosubstitution at the 5-, 10-, or 15-fluoro position. ^1H NMR (300 MHz, $CDCl_3$) δ 9.11–9.03 (m, 2H), 8.88–8.63 (m, 2H), 8.58–8.53 (m, 4H), 3.69–3.64 (m, 2H), 2.49–2.45 (t, J = 6.2 Hz, 2H), 1.87–1.75 (m, 2H), 1.67–1.55 (m, 2H), 0.91–0.85 (m, 2H); ^{19}F NMR (282 MHz, $CDCl_3$) δ −137.17, −137.23, −137.69, −137.72, −140.11, −141.69, −152.66, −152.97, −153.14, −160.54, −160.60, −161.63, −162.03, −162.91. MALDI-TOF *m/z* calculated for $C_{43}H_{20}F_{14}GaN_5O_2$ $[M+H]^+$: 974.065, found: 974.126. UV-Vis (DMSO): λ_{max} (ε) 420 nm (130,300 $M^{-1}\cdot cm^{-1}$).

The gallium corroles were solubilized in DMSO, and concentrations were determined by UV-Vis using calculated extinction coefficients: (**1**) ε_{420nm} = 284,000 $cm^{-1}\cdot M^{-1}$, (**2**) ε_{424nm} = 74,700 $cm^{-1}\cdot M^{-1}$, (**3**) ε_{420nm} = 130,300 $cm^{-1}\cdot M^{-1}$, (**4**) ε_{426nm} = 130,000 $cm^{-1}\cdot M^{-1}$ (Fig. 1). Stock solutions were stored in the dark at room temperature before use.

Table 3. Cytotoxicity of 3 in NCI60 cell panel

Panel/cell line	Growth inhibition, %	Lethality, %
Leukemia		
CCRF-CEM	91.1	
HL-60(TB)	86.1	
K-562	72.9	
MOLT-4	86.0	
RPMI-8226	70.2	
SR	87.5	
Non–small-cell lung cancer		
A549/ATCC	82.7	
EKVX	59.7	
HOP-62	44.9	
HOP-92	81.6	
NCI-H226	61.1	
NCI-H23	64.5	
NCI-H322M	32.9	
NCI-H460	94.2	
NCI-H522	44.6	
Colon cancer		
COLO 205	51.7	
HCC-2998	60.1	
HCT-116	75.5	
HCT-15	57.0	
HT29	60.6	
KM12	80.6	
SW-620	75.9	
CNS cancer		
SF-268	65.8	
SF-295	53.2	
SF-539	85.3	
SNB-75	30.7	
U251	77.4	
Melanoma		
LOX IMVI		9.7
MALME-3M	50.4	
M14	84.1	
MDA-MB-435	90.8	
SK-MEL-2	64.1	
SK-MEL-28		12.1
SK-MEL-5	72.0	
UACC-257	37.2	
UACC-62	91.6	
Ovarian cancer		
IGROV1	55.7	
OVCAR-3	75.9	
OVCAR-4	59.9	
OVCAR-5	53.1	
OVCAR-8	67.3	
NCI/ADR-RES	52.7	
SK-OV-3	32.9	
Renal cancer		
A498	99.0	
ACHN	73.2	
CAKI-1	71.7	
RXF 393	96.7	
SN12C	78.8	
TK-10	47.3	
UO-31	64.7	
Prostate cancer		
PC-3	71.9	
DU-145	64.7	
Breast cancer		
MCF7	63.1	
MDA-MB-231/ATCC	72.5	
HS 578T	81.2	
BT-549	73.0	
T-47D	45.9	
MDA-MB-468	86.3	

Reagents were obtained from the indicated suppliers: HBSS without phenol red and trypsin-EDTA (0.25%), Invitrogen/Gibco; PBS, Mediatech; 4′,6-diamidino-2-phenylindole dihydrochloride (DAPI) and DMSO, Sigma-Aldrich; paraformaldehyde, Electron Microscopy Sciences; WGA, Alexa Fluor 488 conjugate, Invitrogen/Molecular Probes; and ProLong Gold Antifade Mountant with DAPI, Life Technologies.

Human Cancer Cell Lines. Four cell lines from the NCI60 cell panel (44) representing four distinct tumor types were used in this study: DU-145, prostate; MDA-MB-231, breast; SK-MEL-28, melanoma; and OVCAR-3, ovarian. Cells were grown in RPMI 1640 cell culture medium (Mediatech) containing 2 mM L-glutamine, supplemented with 10% FBS (Omega Scientific), and maintained at 37 °C under 5% CO_2 in a humidified incubator.

MTS Assay. Cells (DU-145, MDA-MB-231, SK-MEL-28, and OVCAR-3) were seeded in 96-well microtiter plates (5×10^3 cells per well; 0.09 mL per well) 24 h before the addition of corroles. At the time of drug treatment, stock solutions of **1**–**4** were diluted to 10-fold the desired final test concentrations with RPMI medium 1640. Aliquots of 10 μL of these diluted solutions were added to the appropriate microtiter wells containing 90 μL of medium, resulting in the required final drug concentrations (eight concentrations per compound, ranging from 0.3 to 600 μM). The final concentration of DMSO in test culture was <1%. All cells were incubated in the dark throughout the 72-h exposure period and did not receive prolonged exposure to light. Following 72 h of exposure at 37 °C, cell viability was determined using the MTS assay (CellTiter 96 Aqueous One Cell Proliferation Assay; Promega) according to the manufacturer's instructions. Absorbances were measured using a microplate reader (Synergy 4; Biotek Instruments) at 490 nm. Experiments were performed in triplicate and each dose–response curve represents the mean of three or more independent experiments. Spectrophotometric data were analyzed by sigmoid dose–response, nonlinear regression analysis; the IC_{50}, Hill slope (γ), E_{max} values, and associated SE were calculated using GraphPad Prism 6 (GraphPad Software).

Confocal Imaging of Intracellular Gallium Corroles. Confocal images were obtained for DU-145, MDA-MB-231, SK-MEL-28, and OVCAR-3 cells exposed to 3 μM **1**, **2**, **3**, or **4** for 3 h at 37 °C, 5% CO_2 in the dark using an upright LSM510 2-Photon microscope (Carl Zeiss MicroImaging). Protocols for seeding cells, immunolabeling, and confocal image acquisition were as previously described (41).

Uptake of Gallium Corroles. The intracellular uptake of gallium corroles was quantified using the ImageXpress^{ultra} laser point-scanning confocal microscope (Molecular Devices). The fluorescence image acquisition settings were as previously reported (41). Cells (DU-145, SK-MEL-28, MDA-MB-231, and OVCAR-3) were seeded in 96-well dishes (8×10^3 cells per well in 0.1 mL) and allowed to attach overnight. Compound **1**, **2**, **3**, or **4** was added directly to cell media at 30 μM final concentration or media only control, and incubated for 0.25, 1, 3, or 24 h at 37 °C in the dark under a 5% CO_2 atmosphere. Cells were fixed and labeled in situ with WGA–Alexa Fluor 488 conjugate and DAPI to allow for the identification of cell boundary and nucleus, respectively. The quantification of blue (DAPI) fluorescence signals in each sample yielded the total number of cells in that population. Corresponding determination of red (corrole) fluorescence within each cell, corrected for background fluorescence from untreated cells, provided the number of cells containing corroles. For each corrole concentration at various time points, fluorescence data were obtained for 1,000–22,000 individual cells. Data acquisitions and analyses were performed as described (41). The percentage of corrole-positive cells and the median fluorescence intensity (median RFU) for each treatment were plotted in a three-axis graph using Microsoft Office Excel 2007 (Microsoft Corporation).

NCI60 Anticancer Drug Screen. The aminocaproate-substituted corrole **3** was submitted to NCI for cytotoxic screening at a single high dose (10^{-5} M) in a panel of 60 human tumor cell lines (NCI60) (44, 57). Details of the cytotoxicity assessment in the NCI anticancer drug screen have been described previously (58).

ACKNOWLEDGMENTS. The experimental assistance of Dr. Shane Mangold and software assistance of Dr. Ching Ouyang are gratefully acknowledged. We thank Dr. Brian Armstrong of the Light Microscopy Digital Imaging Core Facility and Dr. Gerald Wuenschell of the Translational Biomarker Discovery Core Facility of the City of Hope Comprehensive Cancer Center for their technical assistance, and the NCI Developmental Therapeutics Program for the 60 cell line screen. This work was supported by a Caltech/COH grant (to J.T. and H.B.G.) and by NIH Grant DK01038 (to H.B.G.).

1. Aviv-Harel I, Gross Z (2009) Aura of corroles. *Chemistry* 15(34):8382–8394.
2. Aviezer D, et al. (2000) Porphyrin analogues as novel antagonists of fibroblast growth factor and vascular endothelial growth factor receptor binding that inhibit endothelial cell proliferation, tumor progression, and metastasis. *Cancer Res* 60(11): 2973–2980.
3. Ethirajan M, Chen Y, Joshi P, Pandey RK (2011) The role of porphyrin chemistry in tumor imaging and photodynamic therapy. *Chem Soc Rev* 40(1):340–362.
4. Palmer JH (2012) Transition metal corrole coordination chemistry. *Molecular Electronic Structures of Transition Metal Complexes I, Structure and Bonding*, eds Mingos DMP, Day P, Dahl JP (Springer, Berlin), Vol 142, pp 49–89.
5. Giordanetto F, Kihlberg J (2014) Macrocyclic drugs and clinical candidates: What can medicinal chemists learn from their properties? *J Med Chem* 57(2):278–295.
6. Driggers EM, Hale SP, Lee J, Terrett NK (2008) The exploration of macrocycles for drug discovery—an underexploited structural class. *Nat Rev Drug Discov* 7(7):608–624.
7. Kotz J (2012) Bringing macrocycles full circle. *SciBX* 5(45):1–7.
8. Yudin AK (2015) Macrocycles: Lessons from the distant past, recent developments, and future directions. *Chem Sci (Camb)* 6(1):30–49.
9. Pisarek S, Maximova K, Gryko D (2014) Strategies toward the synthesis of amphiphilic porphyrins. *Tetrahedron* 70(38):6685–6715.
10. Johnson AW, Kay IT (1965) Synthesis of corroles and related ring systems. *Proc R Soc Lond A Math Phys Sci* 288(1414):334–341.
11. Johnson AW, Kay IT (1964) The pentadehydrocorrin (corrole) ring system. *Proc Chem Soc Lond* 1964:89–90.
12. Johnson AW, Kay IT (1961) The synthesis of derivatives of corrole. An amendment. *Proc Chem Soc Lond* 1961:168–169.
13. Johnson AW, Price R (1960) The synthesis of derivatives of corrole (pentadehydrocorrin). *J Chem Soc* 1960:1649–1653.
14. Gross Z, Galili N, Saltsman I (1999) The First direct synthesis of corroles from pyrrole. *Angew Chem Int Ed* 38(10):1427–1429.
15. Gross Z, et al. (1999) Solvent-free condensation of pyrrole and pentafluorobenzaldehyde: A novel synthetic pathway to corrole and oligopyrromethenes. *Org Lett* 1(4):599–602.
16. Paolesse R, Licoccia S, Bandoli G, Dolmella A, Boschi T (1994) First direct synthesis of a corrole ring from a monopyrrolic precursor. Crystal and molecular structure of (triphenylphosphine)-(5,10,15-triphenyl-2,3,7,8,12,13,17,18-octamethylcorrolato) cobalt(III)-dichloromethane. *Inorg Chem* 33(6):1171–1176.
17. Paolesse R, Tassoni E, Licoccia S, Paci M, Boschi T (1996) One-pot synthesis of corrolates by cobalt catalyzed cyclization of formylpyrroles. *Inorg Chim Acta* 241(2):55–60.
18. Licoccia S, Di Vona ML, Paolesse R (1998) Acid-catalyzed cyclization of 1,19-unsubstituted a,c-biladienes. *J Org Chem* 63(10):3190–3195.
19. Paolesse R, et al. (1999) 5,10,15-Triphenylcorrole: A product from a modified Rothemund reaction. *Chem Commun* 1999(14):1307–1308.
20. Gryko DT (2000) A simple, rational synthesis of -substituted AB-corroles. *Chem Commun* 2000(22):2243–2244.
21. Gryko DT (2002) Recent advances in the synthesis of corroles and core-modified corroles. *Eur J Org Chem* 2002(11):1735–1743.
22. Gryko DT (2008) Adventures in the synthesis of meso-substituted corroles. *J Porphyr Phthalocyanines* 12(08):906–917.
23. Guilard R, et al. (2002) Synthesis of corroles bearing up to three different meso substituents. *Org Lett* 4(25):4491–4494.
24. Paolesse R, Nardis S, Sagone F, Khoury RG (2001) Synthesis and functionalization of meso-aryl-substituted corroles. *J Org Chem* 66(2):550–556.
25. Palmer JH, Durrell AC, Gross Z, Winkler JR, Gray HB (2010) Near-IR phosphorescence of iridium(III) corroles at ambient temperature. *J Am Chem Soc* 132(27):9230–9231.
26. Alemayehu AB, Ghosh A (2011) Gold corroles. *J Porphyr Phthalocyanines* 15(02): 106–110.
27. Rabinovich E, Goldberg I, Gross Z (2011) Gold(I) and gold(III) corroles. *Chemistry* 17(44):12294–12301.
28. Paolesse R (2008) Corrole: The little big porphyrinoid. *Synlett* 2008(15):2215–2230.
29. Aviv I, Gross Z (2007) Corrole-based applications. *Chem Commun* 2007(20):1987–1999.
30. Aviv-Harel I, Gross Z (2011) Coordination chemistry of corroles; with focus on main group elements. *Coord Chem Rev* 255:717–736.
31. Blumenfeld C, et al. (2015) Control of oligomerization and oxidation steps in the synthesis of tris(pentafluorophenyl)corrole. *Eur J Org Chem* 2015(14):3022–3025.
32. Bendix J, et al. (2000) Structural, electrochemical, and photophysical properties of gallium(III) 5,10,15-tris(pentafluorophenyl)corrole. *Angew Chem Int Ed Engl* 39(22): 4048–4051.
33. Saltsman I, et al. (2002) Selective substitution of corroles: Nitration, hydroformylation, and chlorosulfonation. *J Am Chem Soc* 124(25):7411–7420.
34. Saltsman I, Goldberg I, Gross Z (2003) One-step conversions of a simple corrole into chiral and amphiphilic derivatives. *Tetrahedron Lett* 44(30):5669–5673.
35. Weaver JJ, et al. (2004) Gallium(III) corroles. *J Porphyr Phthalocyanines* 08(01):76–81.
36. Sorasaenee K, et al. (2007) Amphiphilic aluminium(III) and gallium(III) corroles. *J Porphyr Phthalocyanines* 11(03):189–197.
37. Liu X, Mahammed A, Tripathy U, Gross Z, Steer RP (2008) Photophysics of Soret-excited tetrapyrroles in solution. III. Porphyrin analogues: Aluminum and gallium corroles. *Chem Phys Lett* 459(1-6):113–118.
38. Kowalska D, et al. (2009) Ground- and excited-state dynamics of aluminum and gallium corroles. *Inorg Chem* 48(6):2670–2676.
39. Agadjanian H, et al. (2009) Tumor detection and elimination by a targeted gallium corrole. *Proc Natl Acad Sci USA* 106(15):6105–6110.
40. Agadjanian H, et al. (2006) Specific delivery of corroles to cells via noncovalent conjugates with viral proteins. *Pharm Res* 23(2):367–377.
41. Lim P, et al. (2012) Differential cytostatic and cytotoxic action of metallocorroles against human cancer cells: Potential platforms for anticancer drug development. *Chem Res Toxicol* 25(2):400–409.
42. Hwang JY, et al. (2011) A mechanistic study of tumor-targeted corrole toxicity. *Mol Pharm* 8(6):2233–2243.
43. Hori T, Osuka A (2010) Nucleophilic substitution reactions of meso-5,10,15-tris(pentafluorophenyl)corrole; synthesis of ABC-type corroles and corrole-based organogels. *Eur J Org Chem* 2010(12):2379–2386.
44. Shoemaker RH (2006) The NCI60 human tumour cell line anticancer drug screen. *Nat Rev Cancer* 6(10):813–823.
45. Teo RD, et al. (2014) A cytotoxic and cytostatic gold(III) corrole. *Chem Commun (Camb)* 50(89):13789–13792.
46. Pope AJ, Bruce C, Kysela B, Hannon MJ (2010) Issues surrounding standard cytotoxicity testing for assessing activity of non-covalent DNA-binding metallo-drugs. *Dalton Trans* 39(11):2772–2774.
47. Levasseur LM, Slocum HK, Rustum YM, Greco WR (1998) Modeling of the time-dependency of in vitro drug cytotoxicity and resistance. *Cancer Res* 58(24):5749–5761.
48. Fallahi-Sichani M, Honarnejad S, Heiser LM, Gray JW, Sorger PK (2013) Metrics other than potency reveal systematic variation in responses to cancer drugs. *Nat Chem Biol* 9(11):708–714.
49. Berenbaum MC (1972) In vivo determination of the fractional kill of human tumor cells by chemotherapeutic agents. *Cancer Chemother Rep* 56(5):563–571.
50. Mitchison TJ (2012) The proliferation rate paradox in antimitotic chemotherapy. *Mol Biol Cell* 23(1):1–6.
51. Richardson D, Baker E (1992) Two mechanisms of iron uptake from transferrin by melanoma cells. The effect of desferrioxamine and ferric ammonium citrate. *J Biol Chem* 267(20):13972–13979.
52. Richardson DR (2001) Iron and gallium increase iron uptake from transferrin by human melanoma cells: Further examination of the ferric ammonium citrate-activated iron uptake process. *Biochim Biophys Acta* 1536(1):43–54.
53. Bickerton GR, Paolini GV, Besnard J, Muresan S, Hopkins AL (2012) Quantifying the chemical beauty of drugs. *Nat Chem* 4(2):90–98.
54. Chitambar CR, Purpi DP, Woodliff J, Yang M, Wereley JP (2007) Development of gallium compounds for treatment of lymphoma: Gallium maltolate, a novel hydroxypyrone gallium compound, induces apoptosis and circumvents lymphoma cell resistance to gallium nitrate. *J Pharmacol Exp Ther* 322(3):1228–1236.
55. Chua MS, Bernstein LR, Li R, So SK (2006) Gallium maltolate is a promising chemotherapeutic agent for the treatment of hepatocellular carcinoma. *Anticancer Res* 26(3A):1739–1743.
56. Tang GY, et al. (2015) An in vitro enzymatic assay to measure transcription inhibition by gallium(III) and H3 5,10,15-tris(pentafluorophenyl)corroles. *J Vis Exp* 2015(97): e52355.
57. Collins JM (2006) The NCI Developmental Therapeutics Program. *Clin Adv Hematol Oncol* 4(4):271–273.
58. Monks A, et al. (1991) Feasibility of a high-flux anticancer drug screen using a diverse panel of cultured human tumor cell lines. *J Natl Cancer Inst* 83(11):757–766.